Applied Physics Letters

RESEARCH ARTICLE | OCTOBER 02 2014

Local impedance imaging of boron-doped polycrystalline diamond thin films

A. Zieliński; R. Bogdanowicz ; J. Ryl; L. Burczyk; K. Darowicki

Appl. Phys. Lett. 105, 131908 (2014)
https://doi.org/10.1063/1.4897346

CrossMark

This article may be downloaded for personal use only. Any other use requires prior permission of the author and AIP Publishing. This article appeared in (citation of published article) and may be found at https://doi.org/10.1063/1.4897346

26 February 2024 08:51:38

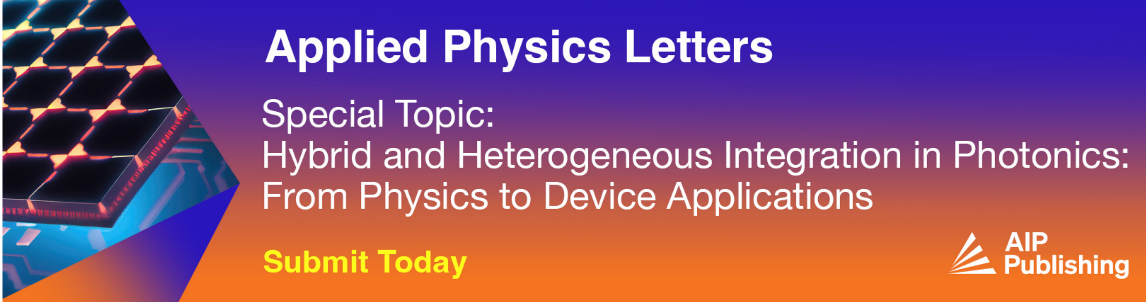

Local impedance imaging of boron-doped polycrystalline diamond thin films

A. Zieliński,[1] R. Bogdanowicz,[2,a)] J. Ryl,[1] L. Burczyk,[1] and K. Darowicki[1]
[1]*Department of Electrochemistry, Corrosion and Material Engineering, Gdansk University of Technology, 11/12 Narutowicza St., 80-233 Gdansk, Poland*
[2]*Department of Metrology and Optoelectronics, Faculty of Electronics, Telecommunications and Informatics, Gdansk University of Technology, 11/12 G. Narutowicza St., 80-233 Gdansk, Poland*

(Received 30 August 2014; accepted 25 September 2014; published online 2 October 2014)

Local impedance imaging (LII) was used to visualise surficial deviations of AC impedances in polycrystalline boron-doped diamond (BDD). The BDD thin film electrodes were deposited onto the highly doped silicon substrates via microwave plasma-enhanced CVD. The studied boron dopant concentrations, controlled by the [B]/[C] ratio in plasma, ranged from 1×10^{16} to 2×10^{21} atoms cm^{-3}. The BDD films displayed microcrystalline structure, while the average size of crystallites decreased from 1 to 0.7 μm with increasing [B]/[C] ratios. The application of LII enabled a direct and high-resolution investigation of local distribution of impedance characteristics within the individual grains of BDD. Such an approach resulted in greater understanding of the microstructural control of properties at the grain level. We propose that the obtained surficial variation of impedance is correlated to the areas of high conductance which have been observed at the grain boundaries by using LII. We also postulate that the origin of high conductivity is due to either preferential boron accumulation, the presence of defects, or sp^2 regions in the intragrain regions. The impedance modulus recorded by LII was in full agreement with the bulk impedance measurements. Both variables showed a decreasing trend with increasing [B]/[C] ratios, which is consistent with higher boron incorporation into BDD film. © *2014 AIP Publishing LLC*. [http://dx.doi.org/10.1063/1.4897346]

In recent years, boron-doped diamonds (BDD) have been extensively investigated because of their remarkable properties. The unique physical and chemical properties enable BDD to be an ideal anode material in electrochemical oxidation,[1,2] biosensing,[3] or electroanalysis.[4] The properties of BDD electrodes, including their lifetime and stability, are significantly determined by their manufacturing process.[5] The structural and electronic properties of boron-doped electrodes have been extensively studied.[6] Moreover, the influence of boron acceptor on surface conductivity,[7,8] morphology,[9,10] and phase structure defined as sp^3/sp^2 ratio,[11–14] was investigated in polycrystalline diamond films.

Liao *et al.*[15] investigated the influence of boron concentration on the structure of diamond thin films for the carrier density ranging from 3.4×10^{17} to 1.8×10^{21} holes/cm^{-3}. It should be noted that the boron-dopant density not only affects the electrical properties of electrode but also its morphological and structural characteristics (sp^3/sp^2 ratio).[16,17] Information about the electrochemical response of BDD electrodes with different boron doping levels can be found in literature.[18] Furthermore, the position and coordination of B dopants in this BDD electrode strongly modify the electronic transport as well as impedance properties.[22] The uptake of boron was found to be non-uniform across the surface of BDD.[19–21] Wilson *et al.*[23] evidenced two different conductivity domains. These local heterogeneities influenced electroactivity of the BDD surface and various electron transfer in $Ru(NH_3)_6^{3+}$. The characterization of these structural defects and boron position is fundamental in understanding the physical and electrochemical properties of BDD electrodes and, in particular, of microelectrode arrays.[24]

Lu *et al.*[22] experimentally measured the variation of local bond length in boron-doped nanocrystalline diamond (B:NCD) films by using spatially resolved STEM-EELS in an aberration-corrected electron microscope. The bond elongation and a significant difference in boron energy-loss near-edge structure have been reported at defective regions in B:NCD grains. In another study, Lu *et al.*[25] demonstrated the presence of B dopant in the diamond lattice as well as the enrichment of B dopant within twin boundaries and defect centres. Turner *et al.*[26] claimed that boron concentrations of ~1 to 3 at. % were found tetrahedrally embedded into the core of diamond grains. The results of Muramatsu and Yamamoto[27] indicate that B atoms in heavily B-doped diamonds form caged B-clusters in the defect space of the diamond lattice.

The majority of earlier investigations focused on the use of advanced surface techniques to elucidate the boron uptake heterogeneity. Nevertheless, the electrochemical performance and AC impedance are typically represented as an average calculated over the whole electrode area. To address the issue of surface heterogeneity, we propose to apply high-resolution local impedance imaging (LII) to visualise spatial deviations of AC impedances on polycrystalline BDD over a wide range of boron dopant concentrations (1×10^{16}–2×10^{21} at. cm^{-3}). To our best knowledge, the direct investigation of local distribution of the impedance properties within the individual grains of BDD films has not yet been reported.

Thus, in this study, we directly investigate AC impedance of hydrogen-terminated thin BDD films synthesized in an microwave plasma-enhanced CVD system (AX5400S, Japan, Seki Technotron) on p-type Si wafers with (111)

a)Author to whom correspondence should be addressed. Electronic mail: rbogdan@eti.pg.gda.pl. Tel.: +48 58 347 1503. Fax: +48 58 347 18 48.

 © 2014 AIP Publishing LLC

26 February 2024 08:51:38
MOST WIEDZY Downloaded from mostwiedzy.pl

orientation. Si substrates were seeded by sonication in nanodiamond suspension (crystallite size of 5–10 nm) for 2 h.[6,7,28] The substrate temperature was kept at 1000 °C during the deposition. The plasma microwave power (@2.45 GHz),[29–31] optimized for diamond synthesis, was kept at 1300 W. The gas mixture ratio was 1% of the molar ratio of CH_4-H_2 at gas volume 300 sccm of the total flow rate. The base pressure was about 10^{-6} Torr, and the process pressure was kept at 50 Torr. The boron level expressed as [B]/[C] ratio in the gas phase was 200, 2000, or 10 000 ppm. Diborane (B_2H_6) was used as dopant precursor. The growth time was 6 h, which resulted in a film of approx. 2 μm thickness. According to the [B]/[C] ratio, the prepared samples were ascribed as AX-BC02k, AX-BC2k, and AX-BC10k.

LII was implemented on the commercial atomic force microscopy (AFM)[32] device (NTegra Prima, Russia, NT-MDT). The combined LII technique is based on a measurement of the current flowing between the sample and the conductive AFM probe. In the case of DC measurement, known as Scanning Spreading Resistance Microscopy (SSRM),[33] an AFM probe is used to perform the local conductivity measurements on the sample surface. Self-designed connection to the conductive probe was installed and coupled with the external impedance system. The clip fixed on the top surface of the sample served as the second electrical terminal (Figure 2(d)). The independent system for electrical measurements consisted of a current-voltage converter (SRS 570, USA, Stanford Research System) and A/D conversion card (NI USB-6356, USA, National Instruments). The additional measuring channel in the card was used to synchronize the acquisition of impedance data with topography. Control and acquisition have been created in LabVIEW (v. 2012, USA, National Instruments). The impedance acquisition was performed in multi-frequency mode; thus, it was possible to extract the modulus and phase images for any investigated frequency. The details of the approach used are given in Ref. 34. The frequency span of perturbation signal equalled 1.6 kHz with 100 mV amplitude. The applied DC bias applied via a conductive probe was equal to 3 V (CDTP-NCHR-10, Switzerland, Nanosensors). The initial contact resistance measured for the described probe type was 2.2 k Ω on gold surface. An analogous technique was used by Hasegawa *et al.*[35] to investigate the transport properties of nanocontacts based on GaAs and InP. O'Hayre *et al.*[40] discussed the details of the contact impedance measurement such as the frequency limits or impedance components.

Furthermore, the bulk impedance amplitude and phase angle spectra were characterized using a custom-built setup.[36–39] The Au needle probes with programmable automatic RCL meter (Fluke PM6306) acted as an impedance analyser in the frequency range from 50 Hz to 1 MHz. The shielded cables were used to reduce a phase error in the high frequency range. The Ohmic contact was made to the BDD surface by using Ti/Pt/Au to average the impedance over the sample area.

The surface morphology and the size of BDD crystallites were investigated with scanning electron microscopy (SEM, S-3400N, Japan, Hitachi). As shown in Figure 1, the dimensions of crystallites decrease with increasing [B]/[C] ratio. The average grain size for the least doped electrode (AX-BC02k) was approx. 2 μm, while for AX-BC10k electrode, it was 4 times smaller. A similar topographical effect was previously reported.[16] It is related to the fact that the addition of boron influences the nucleation process and degenerates the growth of diamond. Lu *et al.* reported that boron mainly accumulates along the grain boundaries of polycrystalline diamond.[22] In the case of AX-BC10k electrode, this phenomenon produces large amounts of a small crystalline agglomerates positioned in-between large crystals (see Fig. 1). In this specific case, SEM gives a relatively low lateral resolution of the electrode morphology compared to the proposed LII technique. Nevertheless, SEM microimages prove that the investigated BDD films fully encapsulate Si substrates without cracks or layer discontinuities, which could cause potential conductivity disturbances.

Figure 2(a) illustrates an example of the spatial distribution of impedance modulus for the highly boron-doped diamond sample (AX-BC10k). For the selected vertical (Fig. 2(b)) and horizontal (Fig. 2(c)) profiles, there are visible conduction heterogeneities between the grains and their boundaries, manifested by changes of 5 orders of magnitude.

The LII spectrum in Figure 2(a) shows the presence of both types of areas, i.e., the conductive areas and fully insulating areas. The "dark" regions corresponding to high impedance regions with approximately 400 kΩ are mostly

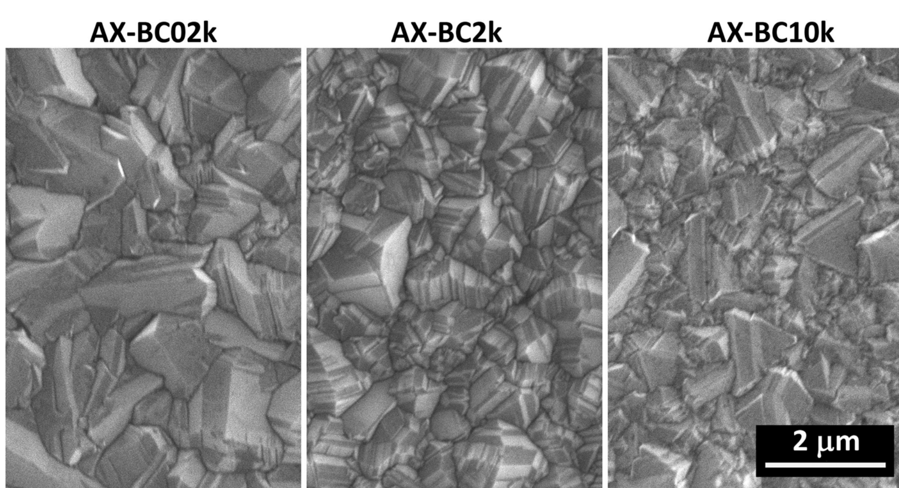

FIG. 1. SEM micrographs presenting the topography of BDD electrodes with different [B]/[C] ratios (200, 2 k, 10 k). Magnification 10 000×.

26 February 2024 08:51:38

MOST WIEDZY Downloaded from mostwiedzy.pl

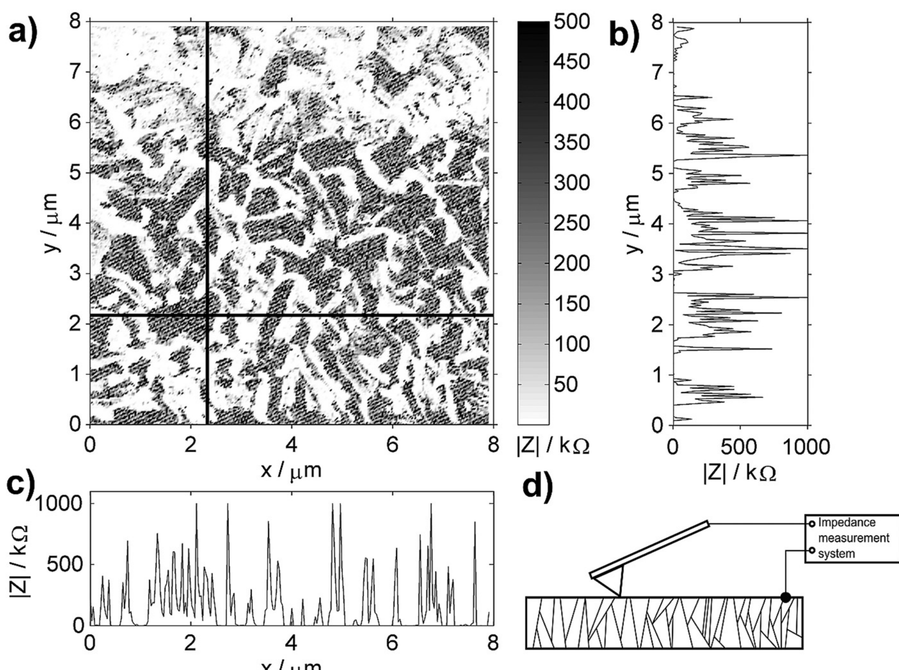

FIG. 2. Image of impedance modulus for the BDD film (AX-BC10k) with 10 k boron content (a). Frequency of impedance spectrum: 1600 Hz. AFM scan in contact mode, velocity 16.19 μm/s, contact force 1.24 μN. Selected vertical (b) and horizontal (c) profiles. Scheme of the electrodes positioned on the sample surface (d).

present on the grain edges or in the intergrain areas. The "white" areas, originating from the intragrain areas or flat surfaces of crystals, are characterized by lower values of impedance, i.e., below 1 kΩ.

In addition, the distribution of increased conductivity areas has been consistently confirmed by pertinent topographic images of the samples tested. This suggests that the contribution of local spreading impedance, assumed to be constant under experimental conditions, predominates over the contact impedance component of the material.

These observations are in agreement not only with the presence of boron between the grains (mostly in the sp^2 phase form) but also inside the grains themselves.[41] Furthermore, it should be mentioned that impedance is not only a function of the sample properties but also of the tip radius (30 nm in this study). The intragrain impedance regions can be burdened with error because the radius of AFM tip does not enable the achievement of surface details.

In a recent study of H-terminated polycrystalline BDDs electrode, Dealouis *et al*. hypothesized that a significant decrease in the local surface conductivity could be explained by a partial passivation of BDD film due to the formation of B–H pairs leading to a decrease in the acceptor levels in the film.[19] Thus, the local impedance measurement allowed the identification of regions with different electrical character, causing the complex electrochemical response of BDDs.

The LII results are presented as the acquired collection of images that have been subjected to decomposition to the form of impedance maps corresponding to one selected measurement frequency. Figure 3 illustrates the surficial distribution of impedance modulus for a frequency of 1.6 kHz. A similar impedance scale was kept for all images presented in Figure 3. The impedance images were recorded for the same value of the bias voltage 3 V, the impedance measurement parameters, area, and topographical scanning speed.

The local impedance images show gradual decrease in the average surface impedance versus boron doping level. The low doped sample AX-BC02k exhibits smooth variation of impedance along the crystal boundaries. The intragrain zones of low impedance become rounded and fuzzy in contradiction to sharp crystal shapes observed in SEM microimages (Figure 1). Furthermore, the inhomogeneous distribution of impedance in the intergrain regions was also observed. This allows for the conclusion that B dopant is not

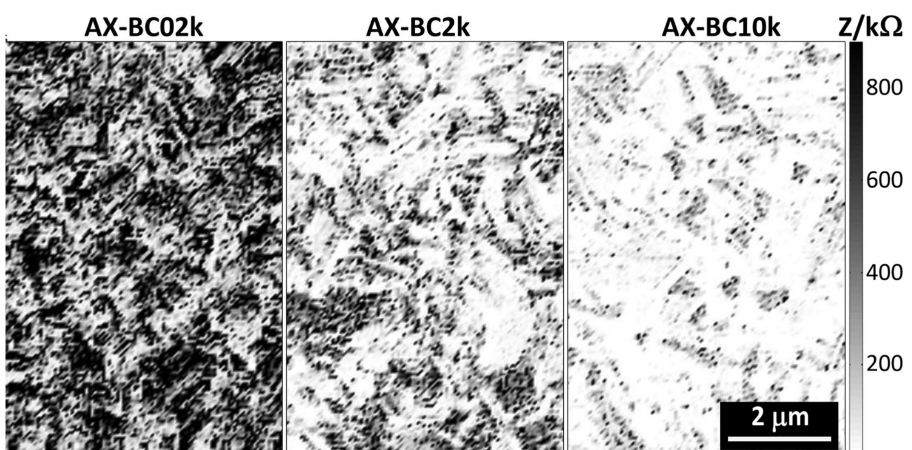

FIG. 3. Impedance modulus maps for three BDD samples arranged according to increasing boron content: 200 (a), 2000 (b), and 10 000 (c). Analysed frequency of impedance spectrum: 1600 Hz. AFM scan in contact mode, velocity 16.19 μm/s, contact force 1.24 μN.

26 February 2024 08:51:38

MOST WIEDZY Downloaded from mostwiedzy.pl

TABLE I. The estimated surface parameters for the set of BDD samples.

Sample	[B]/[C] ratio (ppm)	Boron concentration (at. cm^{-3})	Mean grain size (μm)	Mean surface roughness (nm)	Mean |Z| from LII (kΩ)	|Z| @ 1 kHz (Ω)
AX-BC02k	200	1×10^{16}	1.8	106.23	899	153.6
AX-BC2k	2000	7×10^{19}	1.3	91.85	248	6.06
AX-BC10k	10000	2×10^{21}	0.7	87.35	168	1.15

heterogeneously distributed over the grain. For the highest boron levels (sample AX-BC10k) approaching the metallic transition, the wide conductive zones preferentially formed at the intragrain boundaries. The image of average boron-doped sample (AX-BC2k) demonstrates the combined composition of "white" intragrain zones, characterized by the metallic transition, and "grey" intergrain regions representing semiconducting diamond.

Based on the LII maps shown in Figure 3, the average values of modulus for each BDD sample have been calculated (see Table I). The impedance modulus recorded by LII was in full agreement with the bulk impedance measurements. Both variables showed a decreasing trend with increasing [B]/[C] ratios, which is consistent with higher boron incorporation into BDD film. Moreover, the bulk impedance measurements confirm the tendencies determined by using LII (see Figure 4). These phenomena are most likely linked together since an increase in boron doping level also decreases the percentage of sp^3 hybridized carbon.

It was proposed that the obtained surficial variation of impedance in hydrogen-terminated polycrystalline BDD is correlated with the areas of low impedance that had been observed at the grain boundaries by using LII. The samples with smaller grain size were richer in the grain boundaries containing disordered sp^3 and sp^2 phases. Consequently, the incorporation of defects, including boron dopants was more efficient in these samples.[42] The low impedance is a result of preferential boron incorporation and clustering in the intergrain areas. Moreover, the intergrain regions introduce impurity centres that cause carrier transfer perturbations via various intragrain defects and grain boundaries.

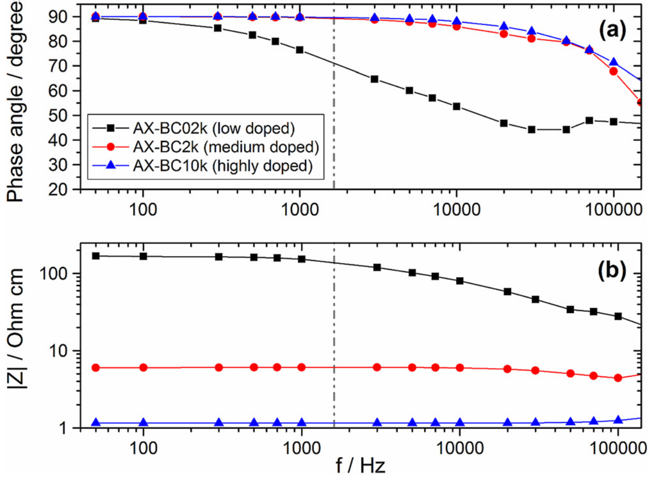

FIG. 4. Bode plots of BDD electrodes with different [B]/[C] ratios in plasma: phase angle (a) and |Z| amplitude (b) vs. frequency. The Ohmic contact and Au needles were applied to BDD electrode.

Similar conclusions have been reached by Wilson *et al.*,[23] who employed conducting atomic force microscopy (C-AFM) with conventional metal-coated AFM probes to provide spatially resolved electrical information on polycrystalline BDD. They reported two different conductivity domains with roughly estimated resistances of ca. 100 kΩ and ca. 50 MΩ linked to the boron dopant levels in individual microcrystalline grains. However, these results had a spatial resolution of about tens of microns. Furthermore, an analogous effect was presented by Bennet *et al.*[43] who investigated how boron dopant accumulates into diamond surface. Based on Raman mapping, they confirmed that boron mainly aggregates at the grain boundaries; the presence of sp^2 carbon increased with increasing boron level.

Figure 4 presents Bode plots obtained for hydrogen-terminated polycrystalline diamond. The bulk impedance modulus and phase angle were recorded at BDD electrodes with Ohmic contacts. For all samples, a gradual decrease in phase angle and modulus plotted against frequency was observed. Moreover, no peaks were registered over a wide frequency range (50–100k Hz), which indicates that only simple capacitive element exists in this model. The grey line in Figure 4 marks the frequency utilized in local impedance images. The authors decided to record images at 1600 Hz due to relatively small differences in phase element in BDDs with different levels of boron incorporation.

It appears that the bulk impedance modulus of highly doped BDD samples is lower than that of low doped sample (Figure 4(b)). The phase angle spectra (Figure 4(a)) showed a continuous decrease down to ca. 40° over 5 kHz only for low doped AXBC02k sample, which results from the impact of resistive behaviour.

In summary, the LII provides considerable insight into the complex nature of BDD as an electrode surface. It was proposed that the obtained surficial variation of impedance correlates with the areas of high conductance observed at the grain boundaries. It was postulated that the origin of high conductivity is due to boron accumulation in the intragrain region. For the selected vertical and horizontal profiles of impedance, the visible conduction heterogeneities between the grains and their boundaries were present as manifested by changes of 5 orders of magnitude. The method can be used on global scale as a technique supplementary to conventional impedance measurements.

This work was supported by the Polish National Science Centre (NCN) under grant No. 2011/03/D/ST7/03541. The DS funds of the Faculty of Electronics, Telecommunications and Informatics and the Faculty of Chemistry at the Gdansk University of Technology are also acknowledged.

26 February 2024 08:51:38

MOST WIEDZY Downloaded from mostwiedzy.pl

[1]M. Panizza, A. Kapalka, and C. Comninellis, Electrochim. Acta **53**, 2289 (2008).
[2]M. Panizza, P. A. Michaud, G. Cerisola, and C. Comninellis, Electrochem. Commun. **3**, 336 (2001).
[3]A. Härtl, E. Schmich, J. A. Garrido, J. Hernando, S. C. R. Catharino, S. Walter, P. Feulner, A. Kromka, D. Steinmüller, and M. Stutzmann, Nat. Mater. **3**, 736 (2004).
[4]P. Gan, R. G. Compton, and J. S. Foord, Electroanalysis **25**, 2423 (2013).
[5]S. K. Johnson, L. L. Houk, J. Feng, R. S. Houk, and D. C. Johnson, Environ. Sci. Technol. **33**, 2638 (1999).
[6]W. Gajewski, P. Achatz, O. A. Williams, K. Haenen, E. Bustarret, M. Stutzmann, and J. A. Garrido, Phys. Rev. B **79**, 045206 (2009).
[7]S. D. Janssens, P. Pobedinskas, J. Vacik, V. Petráková, B. Ruttens, J. D'Haen, M. Nesládek, K. Haenen, and P. Wagner, New J. Phys. **13**, 083008 (2011).
[8]O. A. Williams, M. D. Whitfield, R. B. Jackman, J. S. Foord, J. E. Butler, and C. E. Nebel, Diamond Relat. Mater. **10**, 423 (2001).
[9]S. Gupta, B. R. Weiner, and G. Morell, J. Appl. Phys. **92**, 5457 (2002).
[10]O. A. Williams, M. Nesladek, M. Daenen, S. Michaelson, A. Hoffman, E. Osawa, K. Haenen, and R. B. Jackman, Diamond Relat. Mater. **17**, 1080 (2008).
[11]M. Kahn and W. Waldhauser, Berg- Huettenmaenn. Monatsh. **155**, 534 (2010).
[12]F. Pruvost, E. Bustarret, and A. Deneuville, Diamond Relat. Mater. **9**, 295 (2000).
[13]J. H. T. Luong, K. B. Male, and J. D. Glennon, Analyst **134**, 1965 (2009).
[14]P. Achatz, E. Bustarret, C. Marcenat, R. Piquerel, T. Dubouchet, C. Chapelier, A. M. Bonnot, O. A. Williams, K. Haenen, W. Gajewski, J. A. Garrido, and M. Stutzmann, Phys. Status Solidi A **206**, 1978 (2009).
[15]X. Z. Liao, R. J. Zhang, C. S. Lee, S. T. Lee, and Y. W. Lam, Diamond Relat. Mater. **6**, 521 (1997).
[16]R. Bogdanowicz, A. Fabiańska, L. Golunski, M. Sobaszek, M. Gnyba, J. Ryl, K. Darowicki, T. Ossowski, S. D. Janssens, K. Haenen, and E. M. Siedlecka, Diamond Relat. Mater. **39**, 82 (2013).
[17]J. Czupryniak, A. Fabiańska, P. Stepnowski, T. Ossowski, R. Bogdanowicz, M. Gnyba, and E. M. Siedlecka, Cent. Eur. j. Phys. **10**, 1183 (2012).
[18]G. R. Salazar-Banda, L. S. Andrade, P. A. P. Nascente, P. S. Pizani, R. C. Rocha-Filho, and L. A. Avaca, Electrochim. Acta **51**, 4612 (2006).
[19]C. Deslouis, J. de Sanoit, S. Saada, C. Mer, A. Pailleret, H. Cachet, and P. Bergonzo, Diamond Relat. Mater. **20**, 1 (2011).
[20]M. Tsigkourakos, T. Hantschel, D. K. Simon, T. Nuytten, A. S. Verhulst, B. Douhard, and W. Vandervorst, Carbon **79**, 103–112 (2014).
[21]M. Tsigkourakos, T. Hantschel, C. Bangerter, and W. Vandervorst, "Electrical probing of B-doped diamond seeds embedded into the interfacial layer of a conductive diamond film," Phys. Status Solidi A (published online).
[22]Y.-G. Lu, S. Turner, J. Verbeeck, S. D. Janssens, P. Wagner, K. Haenen, and G. V. Tendeloo, Appl. Phys. Lett. **101**, 041907 (2012).
[23]N. R. Wilson, S. L. Clewes, M. E. Newton, P. R. Unwin, and J. V. Macpherson, J. Phys. Chem. B **110**, 5639 (2006).
[24]A. L. Colley, C. G. Williams, U. D'Haenens Johansson, M. E. Newton, P. R. Unwin, N. R. Wilson, and J. V. Macpherson, Anal. Chem. **78**, 2539 (2006).
[25]Y.-G. Lu, S. Turner, J. Verbeeck, S. D. Janssens, K. Haenen, and G. V. Tendeloo, Appl. Phys. Lett. **103**, 032105 (2013).
[26]S. Turner, Y.-G. Lu, S. D. Janssens, F. Da Pieve, D. Lamoen, J. Verbeeck, K. Haenen, P. Wagner, and G. Van Tendeloo, Nanoscale **4**, 5960 (2012).
[27]Y. Muramatsu and Y. Yamamoto, Diamond Relat. Mater. **39**, 53 (2013).
[28]R. Bogdanowicz, J. Ryl, K. Darowicki, and B. B. Kosmowski, J. Solid State Electrochem. **13**, 1639 (2009).
[29]R. Bogdanowicz, M. Gnyba, P. Wroczyński, and B. B. Kosmowski, J. Optoelectron. Adv. Mater. **12**, 1660 (2010).
[30]R. Bogdanowicz, Acta Phys. Pol., A **114**, A33 (2008).
[31]R. Bogdanowicz, M. Gnyba, and P. Wroczyński, J. Phys. IV France **137**, 57 (2006).
[32]G. Binnig, C. F. Quate, and C. Gerber, Phys. Rev. Lett. **56**, 930 (1986).
[33]P. Eyben, M. Xu, N. Duhayon, T. Clarysse, S. Callewaert, and W. Vandervorst, J. Vac. Sci. Technol., B **20**, 471 (2002).
[34]K. Darowicki, A. Zieliński, and K. J. Kurzydłowski, Sci. Technol. Adv. Mater. **9**, 045006 (2008).
[35]H. Hasegawa, T. Sato, and S. Kasai, Appl. Surf. Sci. **166**, 92 (2000).
[36]J. J. Kopanski, J. F. Marchiando, and J. R. Lowney, Mater. Sci. Eng. B **44**, 46 (1997).
[37]S. V. Kalinin and D. a. Bonnell, Appl. Phys. Lett. **78**, 1306 (2001).
[38]S. V. Kalinin, R. Shao, and D. a. Bonnell, J. Am. Ceram. Soc. **88**, 1077 (2005).
[39]L. S. C. Pingree and M. C. Hersam, Appl. Phys. Lett. **87**, 233117 (2005).
[40]R. O'Hayre, M. Lee, and F. B. Prinz, J. Appl. Phys. **95**, 8382 (2004).
[41]G. Zhang, S. Turner, E. A. Ekimov, J. Vanacken, M. Timmermans, T. Samuely, V. A. Sidorov, S. M. Stishov, Y. Lu, B. Deloof, B. Goderis, G. Van Tendeloo, J. Van de Vondel, and V. V. Moshchalkov, Adv. Mater. **26**, 2034 (2014).
[42]G. Zhang, S. D. Janssens, J. Vanacken, M. Timmermans, J. Vacík, G. W. Ataklti, W. Decelle, W. Gillijns, B. Goderis, K. Haenen, P. Wagner, and V. V. Moshchalkov, Phys. Rev. B **84**, 214517 (2011).
[43]K. E. Bennet, K. H. Lee, J. N. Kruchowski, S.-Y. Chang, M. P. Marsh, A. A. Van Orsow, A. Paez, and F. S. Manciu, Materials **6**, 5726 (2013).

26 February 2024 08:51:38

MOST WIEDZY Downloaded from mostwiedzy.pl